

CO Hydrogenation over functionalized AIMCM-41 materials and ZSM-11/5 zeolites as catalysts

B. Smili^{a,*}, M. Sakmeche^b, A. Belhakem^c, L. Belgacem^d, C. Tabti^c

a) Laboratory of Energy Environment and Information System (LEEIS), Department of Material Sciences, Faculty of Sciences and Technology, University of Adrar, National Highway No. 06. Adrar 01000, Algeria.

b) Laboratory of Saharan natural resources (LRNS), Department of hydrocarbons and renewable energies, Faculty of Science and Technology. University of Adrar, National High way No. 06. Adrar 01000, Algeria.

c) Department of Chemistry, University of Mostaganem, B.P 1001, 27000 Mostaganem, Algeria

d) Research center in industrial technologies CRTI, Cheraga 16014, Algiers, Algeria

Received 8 April 2022; received in revised form 22 May 2022; accepted 24 June 2022 (DOI: 10.30495/IJC.2022.1956221.1928)

ABSTRACT

We studied the reaction in which carbon monoxide is converted to hydrocarbons, and investigated the behaviors and the combination system of catalysts exchanged with platinum and ammonium ions. Experiments were conducted at 1.2 MPa, 523K, and CO/H₂=1 ratio. The structure and the texture of the catalysts, assessed by XRD, BET/BJH, and SEM, exhibited a microporosity for ZSM-5/11 and a micro/mesoporosity for AIMCM-41, which implies a direct effect on the catalytic properties of these materials. The conversions obtained were 60%, 55%, and 50% for Ptⁿ⁺/H⁺-catalysts, Ptⁿ⁺-catalysts, and H⁺-catalysts respectively. Such conversions could be attributed to the good acidity resulting from the simultaneous presence of Ptⁿ⁺/H⁺ at different oxidation states of platinum, which was revealed by XANES PtL_{III} analysis, and their uniform dispersion within the inner surface and its grain size average conducted by the titration of adsorbed H₂-O₂. FTIR analysis showed a better distribution of acid sites for bi-exchanged catalysts over mono-exchanged ones, which resulted in a good catalytic activity. These results suggest a strong correlation between the high selectivity of light hydrocarbon products, the ions, and the catalyst types. These differences depended mainly on the facility of forming different products, such as n/iso-alkanes and alkenes. Skeletal isomerization was the main transformation observed on exchanged catalysts, particularly those with Ptⁿ⁺/H⁺ ions. A deactivation process of catalysts, versus time-on-stream, begins after 70 minutes, especially for combined exchanged materials.

Keywords: AIMCM-41 and ZSM 5/11 Materials; structure and texture; Acidity; Pt+/H+ function; carbon monoxide hydrogenation.

1. Introduction

CO hydrogenation seems to be an advantageous process to obtain clean products and, comply with several environmental regulations [1,2]. To support such regulations, catalytic processes are considered important factors to reduce industrial carbon monoxide emissions compared to those used in cracking units, isomerization, and catalytic reforming [3]. Selections of catalyst types and reaction conditions allow changes in the obtained product distribution. However, in terms of chain growth mechanism, changes in selectivity are

inherent in formed products, catalyst structure/texture, and the type of ions inserted into catalysts. In the CO hydrogenation reaction, the AIMCM-41, ZSM-5, and ZSM-11 materials with their attractive properties (i.e. surface area, acidity strength, distribution of acid sites, and shape selectivity) are used in comparison to supports used elsewhere [4, 5]. Several authors have studied the hydrogenation reaction of CO using materials exchanged with metals and have obtained results of 45% in light products, which is less important than those obtained for our zeolite catalysts. Furthermore, the same observation applies to other catalysts bi-exchanged such as X, Y, L, and Mordenite. The presence of platinum, ammonium, and combined ions resulted in good catalyst performance on Fischer-

*Corresponding author:

E-mail address: smili.billel@yahoo.fr;

billel.smili@univ-adrar.edu.dz (B. Smili)

tropsch CO hydrogenation [6, 7]. CO hydrogenation process has been studied by several authors according to the desired objective, whether it is a conversion into CO₂ [8], a conversion into methanol [5], or a conversion into ethanol. Moreover, The present work revealed a better yield in low hydrocarbons products compared to the literature [9]. Linear formed 1-alkenes were intercepted and converted by the acidic-materials phase. Due to these characteristics, mesoporous molecular materials revealed interesting results in the studied reaction.

ZSM-11 and ZSM-5 molecular sieves, with winding and straight channel systems, respectively, have two-dimensional interconnected 10 rings with a distribution pore average close to 5. However, MCM-41 mesoporous has a one-dimensional channel system with a very large pore and specific areas of both acidity and solid topologies that can make these materials active and selective. Contrarily to AIMCM-41, ZSM-5 and ZSM-11 zeolites have been shown to have selectivity toward linear products. In this study, the catalytic behaviors of different exchanged catalysts in CO conversion were investigated and compared to previous work [10, 11].

2. Experimental

2.1. Catalysts preparation

Materials with different characteristics (**Table 1**) were synthesized according to the procedures described elsewhere [12–14] and the quantities of the reagents are detailed in **Table 2**. The final gels of synthesis materials had the following molar composition:

AIMCM-41: SiO₂:0.1 Al₂O₃:0.5 Na₂O:0.125 TMA: 127 H₂O,

ZSM-5: 0.02 Al₂O₃: 0.5 SiO₂: 8 Na₂O: 0.175 TPA: 3800H₂O,

ZSM-11: 0.015 Al₂O₃: 0.3 SiO₂: 8 Na₂O: 0.15 TBA: 2700.

All Solids were exchanged with NH₄OH solution and impregnated with platinum solution (PtCl₄, 5H₂O). The (Pt⁺/H⁺)-materials form was obtained by first exchanging them with NH₄OH and then impregnating them with a (PtCl₄, 5H₂O) solution. H-forms were obtained by heating exchanged catalysts at 623K for 8 h to evacuate NH₃. Before reactions, solids were extruded into crystallites of 1 mm and then calcined under airflow (20 mL.min⁻¹) at 523 K for 6 h. The temperature was then raised and fixed at 773 K for 10 h. The platinum and ammonium ion content of materials-based catalysts were 2.5 wt% and 95%, respectively.

2.2. Characterization Methods

The phase analysis of the prepared catalysts was carried out by X-ray diffraction (XRD, Philips PW1830) at

room temperature, using Cu-K α radiation with a corresponding wave-length of 1.54178 Å. The microscopic structure was investigated by means of scanning electron microscopy (SEM, JEOL 6300) operating at 25 keV. The measurement of the specific surface area and average pores diameter were realized on Micromeritics ASAP2020 equipment; the specific surfaces were estimated according to the Sorption methods as BET/BJH methods which were applied to determine an internal surface and particle size. Results of as-synthesized and calcined catalysts are given in **Table 1**. The Lewis and Bronsted acid sites were determined using the IR method by the absorption of pyridine on the surface of the catalysts. Elementary analyses were carried out by atomic absorption with different lamps corresponding to different element compositions. The titration by adsorption of H₂-O₂ was performed to determine the probable metallic dispersion [15]. The catalyst was reduced for 2.5 minutes at 350 °C under H₂ flow, with a 1-hour intermediate stage at 150 °C. Next, the catalysts were cooled under hydrogen flow, and the cell was purged at 25°C under N₂ flow. Pulses of O₂ were repeatedly injected into the catalyst bed until no further consumption of O₂ was observed. The total volume of O₂ was then calculated by summing up the proportions of all the pulses consumed. The platinum X-ray absorption near edge structure (XANES) technique was applied to identify platinum oxidation states. A storage ring works with electron energy at 1.85 GeV and a current between 260 and 360 mA. A beamline placed after a bending magnet equipped with a double crystal monochromator and double borosilicate mirrors for the rejection of harmonics was used for the PtLIII-edge technique. Measurements were done in fluorescence mode using a multi-detector element. This mode was used at the PtLIII edge [13]. Each spectrum was recorded twice with a step of 2 eV (from 11520 to 11600 eV) and 5 s/point, with the estimated energy resolution of the monochromator being approximately 3 eV. The energy/angle calibration, which was performed using various representative model compounds of the coordination chemistry of Pt, was investigated, including metallic Pt foil (thickness of 7.5 mm), k₂PtCl₆, and PtO₂ as references. After sieving, particles in the 100-200 mm range were loaded and agglomerated into a sample holder. The PtLIII-edge was recorded at 25°C under 1 bar of N₂ [16, 17].

2.3. CO hydrogenation reaction

The reaction of the CO hydrogenation process was carried out in a continuous-flow system using a stainless steel reactor with a fixed bed with 8 mm external

Table. 1 : Elemental analysis of different catalysts

Matérials	TO ₂	Na ⁺ before exchange	Acidity at 523K		Pt Loading		Carbon deposition at 523K
			Bronsted	Lewis	D _{Pt} (%)	Pt Wt% by AA	Carbon formation mg C/g _{cat}
Na ⁺ -AIMCM-41	Na ⁺ _{0.0120} (Al _{0.0120} Si _{0.130})O ₂	/	12	47	/	/	10
Na ⁺ -ZSM-5	Na ⁺ _{0.086} (Al _{0.086} Si _{0.90})O ₂	/	15	51	/	/	9.3
Na ⁺ -ZSM-11	Na ⁺ _{0.081} (Al _{0.081} Si _{0.90})O ₂	/	16	40	/	/	8.8
Pt ⁿ⁺ -AIMCM-41	Pt ⁿ⁺ _{0.0050} Na ⁺ _{0.0070} (Al _{0.0120} Si _{0.13})O ₂	0.007	18	55	39	2.413	5.6
Pt ⁿ⁺ -ZSM-5	Pt ⁿ⁺ _{0.034} Na ⁺ _{0.052} (Al _{0.086} Si _{0.90})O ₂	0.052	21	59	30	1.918	4.8
Pt ⁿ⁺ -ZSM-11	Pt ⁿ⁺ _{0.032} Na ⁺ _{0.049} (Al _{0.081} Si _{0.90})O ₂	0.049	22	58	31	2.218	5.2
H ⁺ -AIMCM-41	H _{0.00311} Na ⁺ _{0.0089} (Al _{0.0120} Si _{0.13})O ₂	0.0089	17	53	/	/	6.3
H ⁺ -ZSM-5	H _{0.082} Na _{0.004} (Al _{0.086} Si _{0.13})O ₂	0.004	20	56	/	/	5.9
H ⁺ -ZSM-11	H _{0.077} Na ⁺ _{0.004} (Al _{0.081} Si _{0.13})O ₂	0.004	21	55	/	/	6.1
(Pt ⁿ⁺ , H ⁺)-AIMCM-41	(Pt ⁿ⁺ /H) _{0.011} Na ⁺ _{0.001} (Al _{0.0120} Si _{0.130})O ₂	0.001	21	58	33	2.312	3.5
(Pt ⁿ⁺ , H ⁺)-ZSM-5	(Pt ⁿ⁺ /H) _{0.083} Na ⁺ _{0.003} (Al _{0.086} Si _{0.130})O ₂	0.003	23	61	25	1.716	3.1
(Pt ⁿ⁺ , H ⁺)-ZSM-11	(Pt ⁿ⁺ /H) _{0.078} Na ⁺ _{0.003} (Al _{0.081} Si _{0.130})O ₂	0.003	23	60	28	1.811	3.2

Table. 2: The quantities (% mole percent) of reagents and conditions used in the synthesis of materials.

Réactifs and conditions	% mole percent		
	ZSM-5	ZSM-11	AIMCM-41
Sodium aluminate (Aluminium source)	0.02	0.015	0.1
Silica gel (silicon source)	0.5	0.3	1
Sodium hydroxide (Sodium Oxide source)	16	16	1
H ₂ O	3800	2700	127
TMAOH	/	/	0.125
TPAOH	0.175	/	/
TBABr	/	0.15	/
Crystallization Temperature	115 °C	130 °C	90 °C
Crystallization Time	48h	36h	24h

diameter and 6 mm internal diameter. Prior to reaction tests, catalysts were extruded in the form of vermicelli with a mixture of 5% bentonite clay then cut into 1µm pieces and placed between two layers of inert quartz in ratio 1:1:1:1:1 (Q: C: Q: C: Q) proportion, in the reactor (**Fig. 1**). The Gas Chromatograph Phase connected to the reactor in real-time was used to analyze the obtained products directly. Before reaction, materials were submitted to hydrogen reduction: 50 mL/min at 400 K for 4 h. Catalytic tests were carried out, using 3g of the pre-treated solid, at 523K, 2.1MPa, H₂/CO=1 ratio, and CO space velocity of 0.9 L.h⁻¹ per gram of catalyst. Various periods on stream were used in the tests.

Reaction products were analyzed using a gas chromatograph coupled with Mass spectrometry (HRGC-5300/PerkinElmer clarus-600) equipped with a thermal conductivity detector, a programmed heating element, and a chromatographic column with a length of 3m, a diameter of 4mm, filled with fused silica and WCOT Al₂O₃/KCl. The hydrocarbon results were analyzed simultaneously with GC/MS [18] and their distributions were presented directly as a percentage of the number of carbon products, and then selectivities were determined by the following formula:

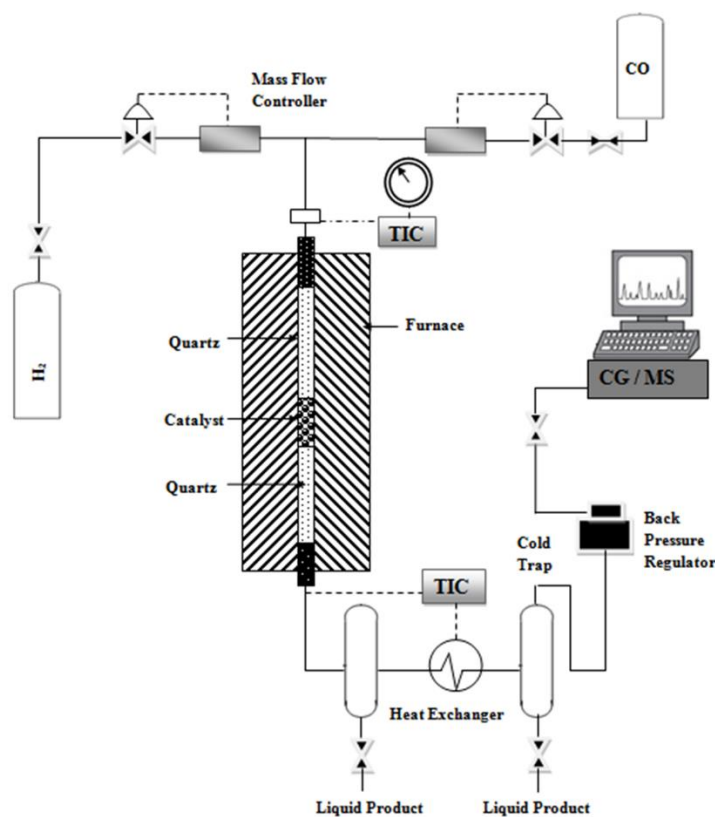


Fig. 1. Schematic diagram of the catalyst test system and used reactor.

$$\frac{\text{Carbon converted to a given product}}{\text{Total Carbon converted}} \quad [19]$$

3. Results and Discussion

3.1. Catalysts characterization

As shown in **Fig. 2**, the characteristic diffraction peaks of ZSM-5 and ZSM-11 molecular sieves appeared between 2θ angles which correspond to 5-40 range. The peaks are probably the same as the intensity of the hierarchical pore molecular sieve. The peaks are broadened, which is often seen in the synthesis of nanomaterials. This means that the grain size of the material was significantly reduced, the crystallinity is relative, and its long-range orderliness will be affected to a certain extent. In Pt/AlMCM-41, the characteristic diffraction peaks of Pt/AlMCM-41 can be observed in previous research [13], with the intense peak toward $2\theta = 2^\circ$, indicating that the synthesis mesoporous materials have good crystallinity with amorphous surface compared with Pt/ZSM-5 and Pt/ZSM-11. In the spectrum of Pt/ZSM-5/11, it can be seen that the incident angle is $2\theta = 38-40^\circ$. The characteristic diffraction peak is attributable to the Pt (111) crystal

plane [20], indicating that the Pt state is formed on the three Pt nanoparticles. Instead, the peak intensity of Pt is different, which may be related to Pt in distinctive valence states. Conversely, in the MCM-41 Pt catalysts, the intensity was reduced while the mesoporous structure was conserved [13, 21, 22].

The exchange of materials with different ion types and the ($\text{Pt}^{n+}/\text{H}^+$) system resulted in a considerable reduction in the surface area of the catalysts. This concomitant loss of sorption capacity of N_2 and XRD observations suggests structural modification in the structure and texture of the materials. The catalyst structure showed a relatively low-surface area (**Table 3**). After calcination, there was a 10% reduction in the intensity of XRD peaks. This is most likely owing to the partial crystalline and organization collapse induced by the presence of platinum in the frameworks with different oxidation states and/or ammonium ions.

The $\text{H}_2\text{-O}_2$ titration measurements revealed a homogenous distribution of the metallic platinum. Mean dispersion of platinum D_{Pt} was calculated using the pulsed-flow technique as shown in **Table 1** while the Pt Wt% was determined by atomic absorption, which confirms the engagement of platinum on the surface of the catalysts [23]. Measurement of the Pt dispersion of

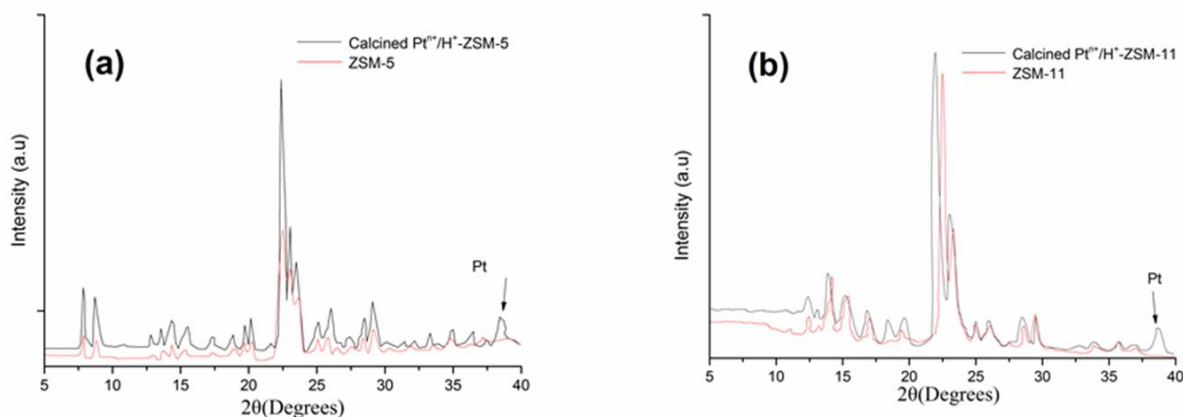


Fig. 2. XRD patterns of ZSM-5(a) and ZSM-11(b).

Table. 3: Structural and textural properties of different catalysts.

Solids	DPA (Å)	Surface area (m ² /g)	Pore Wall thickness
Na ⁺ -AlMCM-41	30	994	9.0
Na ⁺ -ZSM-5	5	324	/
Na ⁺ -ZSM-11	5	375	/
Pt ⁿ⁺ -AlMCM-41	29	970	9.4
Pt ⁿ⁺ -ZSM-5	4.9	322	/
Pt ⁿ⁺ -ZSM-11	4.8	370	/
H ⁺ -AlMCM-41	28	954	9.7
H ⁺ -ZSM-5	4.7	318	/
H ⁺ -ZSM-11	4.7	361	/
Pt ⁿ⁺ / H ⁺ -AlMCM-41	25	879	10.1
Pt ⁿ⁺ /H ⁺ -ZSM-5	4.2	318	/
Pt ⁿ⁺ , H ⁺ -ZSM-11	4.2	358	/

ZSM-11/5 revealed that D_{pt} has decreased relative to that of the AlMCM-41. This slight decrease of D_{pt} confirms a good homogeneous distribution of Pt species in the amorphous surface of AlMCM-41 compared to ZSM-5/11 despite the degree of Pt loading being virtually the same for all of the catalysts (2.5Wt%) [24], knowing that the average diameter of the metallic surface is 0.34 nm with a surface area of 107 m²/g_{catalyst} according to Van Hardeveld and Hartog relation [13, 22]. XANES studies showed that Pt L_{III}-XANES spectra are similar to those observed for model

compounds references PtO₂. Intensities of the Pt L_{III}-absorption edges was intense and centered about 11567.5 - 11569.2 eV for AlMCM-41, 11564.1 - 11566.3 eV for ZSM-5 and 11565.9 - 11567.8eV for AlMCM-41, ZSM-11, there was a low shift observed ($\Delta E \sim 2$ eV) for each catalyst. This could be attributed to an increase in the number of electrons, and thereby a decrease in valence, which suggests a platinum reduction (Pt⁴⁺ to Pt (Fig. 3)). Consequently, platinum is mainly in tetravalent and bivalent forms, with a small amount of metallic Pt. Other reduced or oxidized Pt-

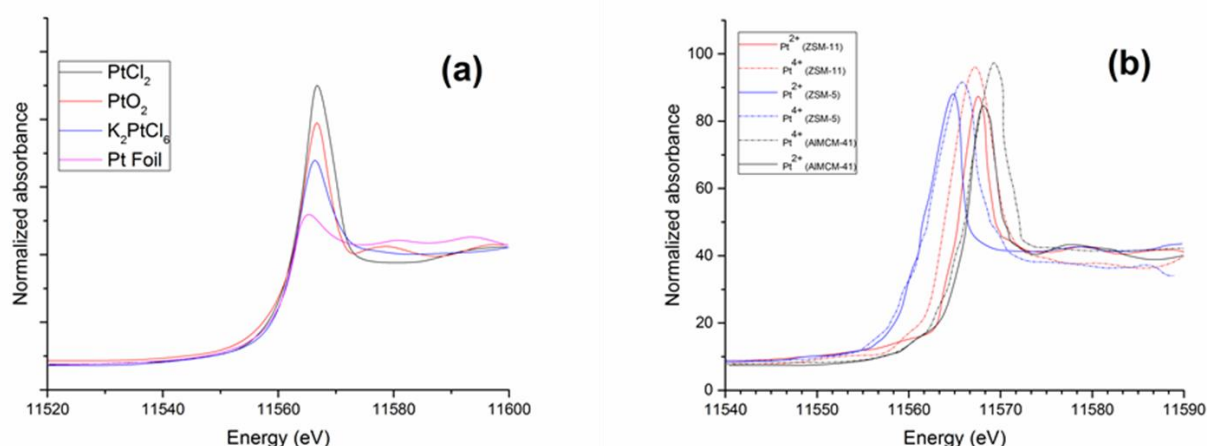


Fig. 3. XANES spectra of the reference materials PtCl₂, PtO₂, K₂PtCl₆, Pt Foil (a) and different oxidation states (Pt²⁺:Pt⁴⁺) of Pt⁺/H-catalysts at 523 K (b).

species, such as Pt⁽⁰⁾ or Pt⁶⁺, were not detected in significant amounts (concentrations less than 3 %).

During the simultaneous reduction with H₂ and carburization pre-treatment of Ptⁿ⁺-catalysts, and mainly after the CO treatment, a change in the Pt ionic form proportion was observed. Then, platinum-phase compositions remained unchanged. This could suggest that the conversion to metallic platinum or carbides seems to be difficult. Previously, similar results for metal-impregnated materials were reported [25]. Considering the reduction behavior of platinum and changes in surface area, crystallinity, and mesoporosity order, the formation of a platinum compound by reaction with the support cannot be excluded.

Catalyst acidities were investigated by pyridine adsorption FTIR technique and ammonia thermo-programmed desorption (NH₃-TPD). The FTIR results obtained from synthesis samples confirm the main bands, which extend to the MCM-41 zeolite and the ZSM-5 and ZSM-11 zeolites (**Fig. 4a, b, c**) and (**Table 1**). A higher number of Lewis acid sites and strong Brønsted acidity were detected for ZSM-5 and ZSM-11 over AIMCM-41 with the same overall profile distribution [22,26].

3.2. CO hydrogenation

Contrarily to the low activity observed for H-catalysts, Ptⁿ⁺ and (Ptⁿ⁺/H⁺) catalysts gave a rise to 35 % CO conversion. As shown in previous studies with iron-catalysts [27], these results could be attributed to the presence of platinum and its ionic states and combination ions, which generated good acidities and affected catalytic performances and selectivities, represented by C_n/C₃ (**Fig. 5**). Due to the important

surface area offered by AIMCM-41, higher methane proportions were obtained for these catalysts. The dissociation of CO during the first step of the reaction results in the formation of a carbide and a surface oxide. Because hydrogen has a higher surface coverage than CO in nebular-type conditions (H₂ > 0.95), hydrogenation reaction with the presence of H₂ permits the oxide to be removed with H₂O formation. Then total hydrogenation of the surface carbon produces CH₄. These species of C-O could then participate in chain-growth mechanisms. The carbon deposition takes place after the catalytic reaction at T = 523K and it is calculated concerning the initial mass of the catalysts engaged in the hydrogenation of the CO. It has been found that the carbon deposit is greater in the case of the monolayer Pt⁺-catalysts and Na⁺-catalysts, which are of the orders of 6.3 to 10 C mg/g_{cat}, respectively, and it is less remarkable for the Pt/H bi-catalysts exchanged which does not exceed 3.5 cmg/g_{cat} (**Table 3**).

As shown in **Fig. 6**, C₂-C₃ ratios of alkenes/alkanes ratios indicate higher alkene selectivity for solids exchanged with platinum and combined ions than those exchanged only with ammonium. Then, catalysts exhibited a higher ethylene/ethane ratio with a lower propylene/propane ratio. A higher proportion of the former ratio was noticed for zeolites compared to mesoporous. The deposition and evolution of the electronic properties of platinum induce variations in intrinsic catalyst properties and consequently influence their catalytic behavior. Indeed, hydrogen is adsorbed in the vicinity of metal particles as well, which contributes to an "extension" of the reactive domain where the reactions take place. The observed differences might probably be explained by the OH group density as well as by the "H" surface diffusivity. In order to highlight

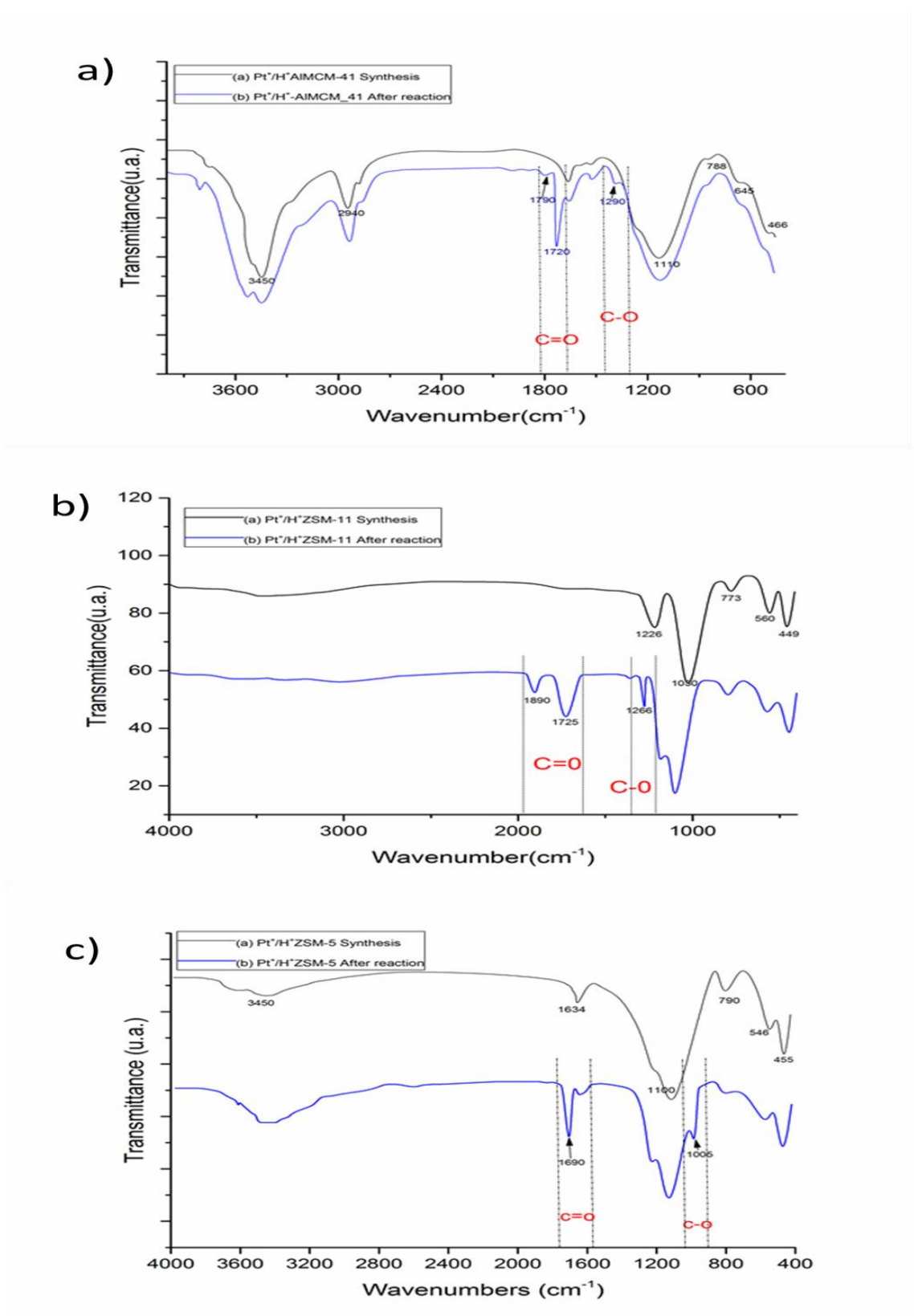


Fig. 4a. FTIR of Pt/HAIMCM-41 catalyst (a) and Pt/H-AIMCM-41 after reaction of CO Hydrogenation (b). **4b.** FTIR of Pt/H-ZSM-11 catalyst (a) and Pt/H-ZSM-11 after reaction of CO Hydrogenation (b). **4c.** FTIR of Pt/H-ZSM-5 catalyst (a) and Pt/H-ZSM-5 after reaction of CO Hydrogenation (b).

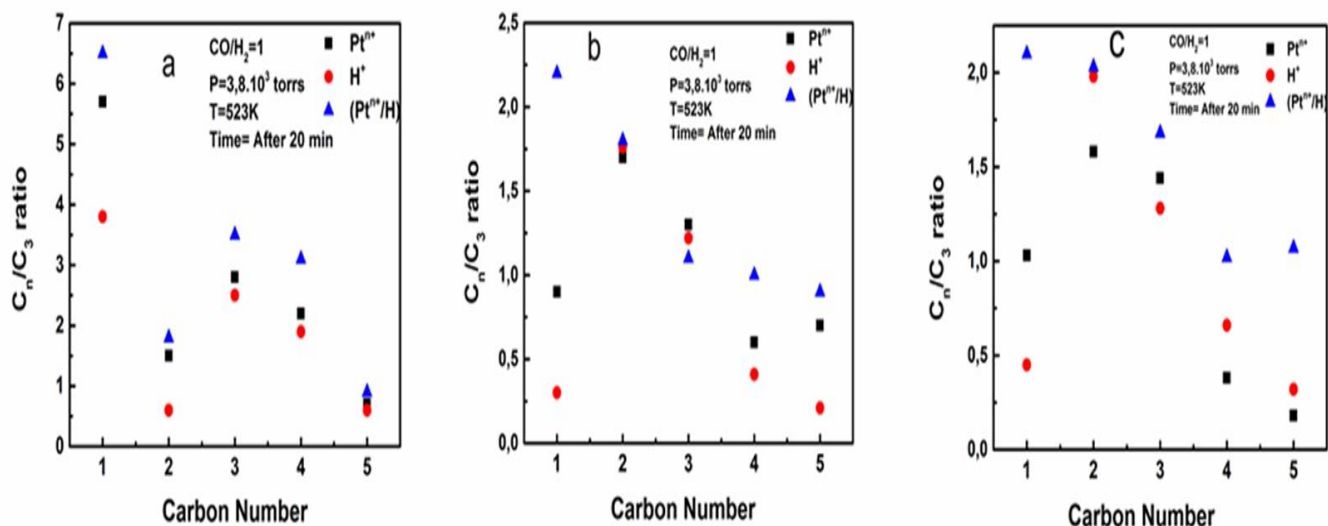


Fig. 5. Distribution of hydrocarbons over exchanged catalysts (a)AlMCM-41, (b)ZSM-11,(c)ZSM-5 after 20min at 523K, P=1,2 MPa, CO/H₂=1.

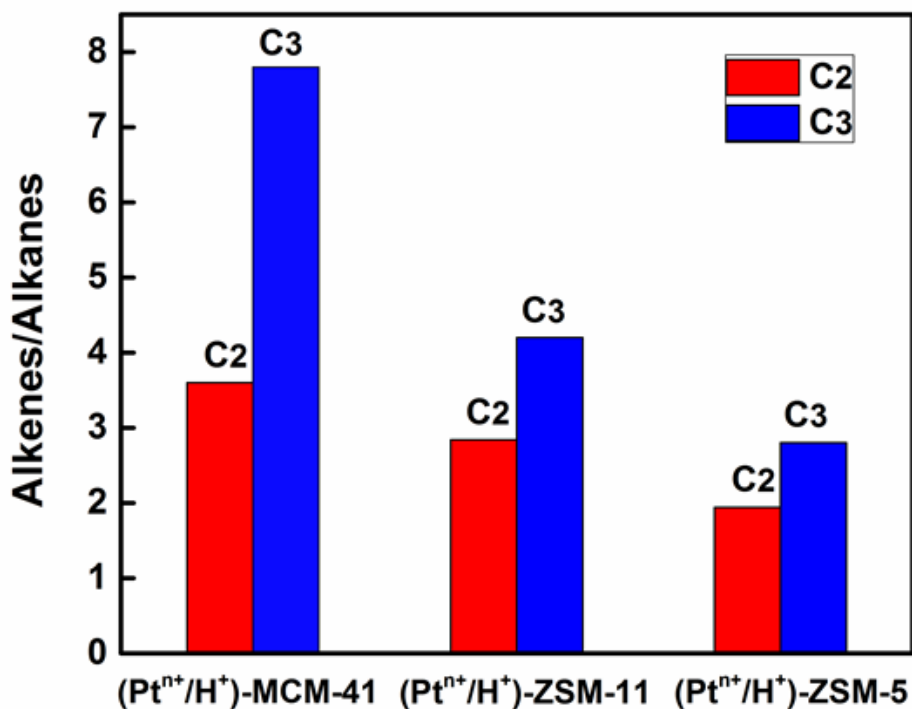


Fig. 6. C₂-C₃ ratios of Alkenes/Alkanes fractions on hydrogenation of CO over different catalyst at 523K, P=1,2 MPa, CO/H₂=1. the exact role of surface diffusion, some research recommends using isotopic exchange experiments intended for H mobility measurement [17]. However, secondary alkene hydrogenation could occur with the present catalysts due to the difference in conversion rates. Higher alkene selectivity should be expected for lower CO conversion. This could be due to the

oligomerization of propylene into other hydrocarbons with the oligomers and cracking on different acid sites [28].

Results obtained from FTIR analysis of Al-MCM-41, ZSM-5 and ZSM-11 (Fig. 4a, b, c) have clearly shown that there is the formation of C=O at 1690, 1720, 1725, 1790 and 1890 cm^{-1} and formation of C-O bands at 1005, 1266 and 1290 cm^{-1} in the interval domains obtained after reaction of CO hydrogenation (Table 4). The absence of the 2600 cm^{-1} band corresponding to the formation of a Pt-O bond for catalysts proves that this band was not formed. This effect could be due to the physical interactions generated by the wt% of platinum ions introduced and the species created with different coordinations, which may generate new active sites. This requires the activation of carbon-hydrogen bonds by an induced polarization phenomenon between materials and the present ions. Consequently, for Pt⁺/H⁺-catalysts, we observed an important formation of methane, a notable increase in C₃ fraction, and a low ethylene/ethane ratio. It seems that propylene was hardly formed on H-catalysts. Changes in activities and material selectivity can be attributed to a number of

factors: pore size, internal surface area, metal oxidation states and acidities.

Fig. 7 shows SEM images of the Pt/H catalysts AlMCM-41 (a), Pt/H-ZSM-11 (b), and Pt/H-ZSM-5 (c). It can be seen from the photos that the porous catalysts Pt /H- have a spherical or nearly spherical microstructure and mesostructure, the diameter of the microspheres is about 1 μm , 1.2 μm , and 3 μm respectively, and the surface is relatively rough. Thus, the molecular sieve surface of ZSM-5 and ZSM-11 has actually a rigid foam-like structure, which is similar to the structure of the product obtained using TPAOH and TBuAOH structuring agents. This indicates that the formation of channels in the Pt/ZSM-5 catalytic structure and ZSM-11 is not formed by the self-assembly of the TPAOH used since the TPAOH is applied as a support template, which resists the formation of the micropores during the molecular sieve crystallization process. The Pt/H- AlMCM-41 shows an occupied mesoporous space, and the void left after the activation forms a micro/mesoporous structure resembling a rigid sponge.

Table 4: Assignments of the different IR bands for the catalysts AlMCM-41, ZSM-5/ZSM-11.

catalyst	Vibrations	Bands	Corresponding bands
Pt ⁺ /H ⁺ -AlMCM-41	3450 cm^{-1}	(O-H)	The formation of platinum complexes in the silica micelle and template
	2940 cm^{-1}	(C-H)	Vibrations of the surfactant molecules
	1622 cm^{-1}	(Si-OH)	The Si-OH deformational vibrations of adsorbed molecules
	1110 cm^{-1}	(Si-O)	assigned to internal and external asymmetric Si-O stretching modes
	788 and 645	(Si-O)	The internal and external asymmetric Si-O stretching modes, and Si-O group
	466 cm^{-1}	(Si-O)	Attributed to tetrahedral Si-O bending modes
	1790 and 1720 cm^{-1}	(C=O)	Band formed after CO hydrogenation reaction
	1290 cm^{-1}	(C-O)	Band formed after CO hydrogenation reaction
Pt/H-ZSM-(5 and 11)	3450 cm^{-1}	(O-H)	The siloxane and/or hydroxyl groups formed by water molecules physisorbed to the surface
	1634 cm^{-1}	(Si-OH)	Deformational vibrations of water molecules
	1100, 1225 cm^{-1}	(Si-O and Si-O-T(Al or Si))	The external and internal asymmetric stretching of the siloxane groups and stretching of Si-O-T
	790, 773	Si-O	The symmetric stretching of the siloxane groups
	546, 560, 455, 449	(Si-O)	The internal flexions of the tetrahedrons correspond
	1690, 1725 and 1890 cm^{-1}	(C=O)	Band formed after CO hydrogenation reaction
1005 and 1266 cm^{-1}	(C-O)	Band formed after CO hydrogenation reaction	

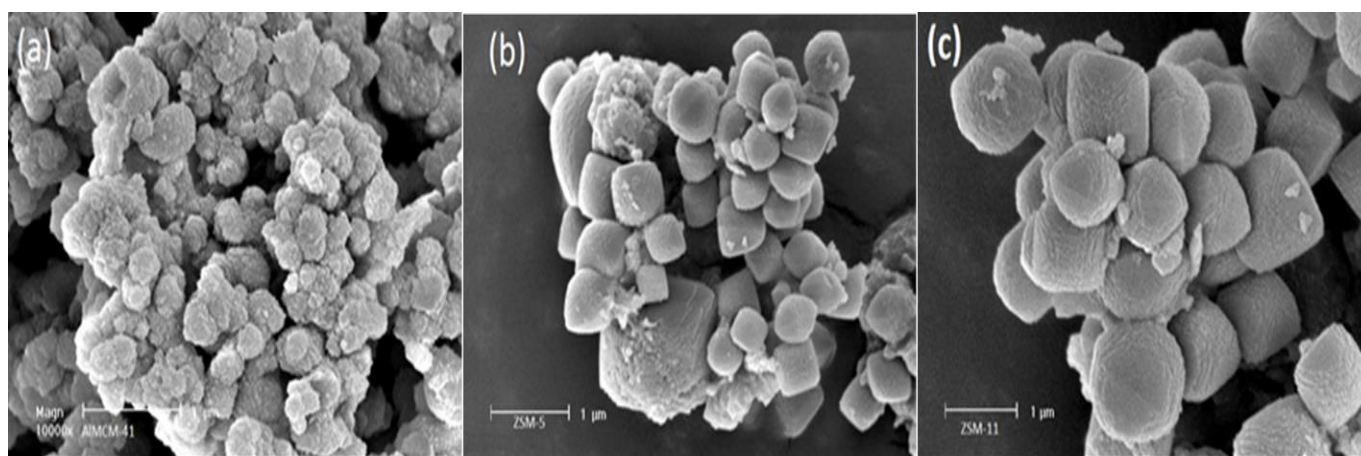


Fig. 7. SEM images of Pt/H-Catalysts (a) AIMCM-41, (b) ZSM-5 and (c)ZSM-11 at 523K.

3.3. Effect of ion exchange

As seen in **Fig. (8 and 9)**, the maximum conversions were observed at around 60%, 55%, and 50% for AIMCM-41, ZSM-11, and ZSM-5, respectively. Their behavior depends strongly on their preparation, pre-treatment and reaction conditions [12, 29, 30]. Since the pre-treatment did not completely carburize the catalyst, the initial rise in activity could be due to the ions' transformation continuing. After 60 minutes of reaction time, deactivation was observed, due to the formation of high-molecular-weight hydrocarbons and deposition of coke, which affect catalytic activities.

This reaction type is exothermic, and heat transfer effects can appear. This can be attributed to thermal exchanges, which were more marked in catalysts swapped with Pt^{n+} and (Pt^{n+}/H^+) ions, probably related to electrostatic fields generated by the presence of several ions, especially the valence states of platinum, as well as to interactions created between these ions and solid surfaces. Recent tests performed using FAPO-11, AIPO, SAPO-11, NaY, LTL, Co-MnO_x, α -Al₂O₃ and clay materials under similar reaction conditions have shown CO conversions to be lower than those found in this investigation [9, 19, 27, 31, 32]. Concerning differences in CO conversion between exchanged catalysts with different forms, it is possible that reactions taking place on the acid sites in the case of two types of catalysts could result in different thermal balances, affecting catalyst behavior directly.

The simultaneous presence of ammonium and platinum ions demonstrated good CO conversion activities and, as a result, good product yields. Then, conversions with (Pt^{n+}/H^+) -catalysts have better catalytic activity than those observed for Pt^{n+} and H^+ -catalysts (**Fig. 9**). In both cases, the reaction environment is different. Contrarily to the exchange with ammonium, the exchange with Pt^{n+}

and (Pt^{n+}/H) permits the appearance of significant concentrations of water and hydrocarbons related to acidity strength generated by ion types.

The catalytic feature of present supports is characterized by the formation of long-chain hydrocarbons (wax), which can be related to uniform pores. For (Pt^{n+}/H) -catalysts, products will have a longer residence time in catalyst particles, favoring hydrocarbon chain growth. As shown in **Fig. 9**, which represents the alkenes/alkanes ratio, the most pronounced difference is observed for the combined exchange catalyst compared to others with low C₃ and C₂ ratios (**Fig. 5, 6**). The aim of the bifunctional exchange is to take advantage of possible synergetic effects between the two ions and thus produce a highly active, selective, and stable catalyst.

Contrary to that observed for the exchange with Pt^+ or Pt^{n+}/H^+ ions, the H-catalysts exhibit a relatively low CO conversion with only a 20% rate of obtained products. A slight increase in these product fractions was noticed for zeotype (AIMCM-41) than for zeolites (ZSM-11 and ZSM-5) (**Fig. 8**). These results could be attributed to the low participation of these ions in CO hydrogenation, which generated a low acidity compared to Pt^{n+} - and (Pt^{n+}/H^+) -catalysts and may alter the binding energy and the adsorption capability of the reactive molecules. On the other hand, these ions don't cover all the surface, which consequently permit reactants' access to active sites and generates higher hydrocarbon products. The exchange with ammonium influences the kinetics and energetics of the adsorption of different reactants on different catalyst surfaces. The surfaces of zeolites were lowly covered due to their structures, resulting in limited hydrocarbon distributions.

Due to their structure and texture (**Table 3**), zeolites favor the formation of linear products. Then, the iso-alkenes/n-alkanes ratio was more favored by

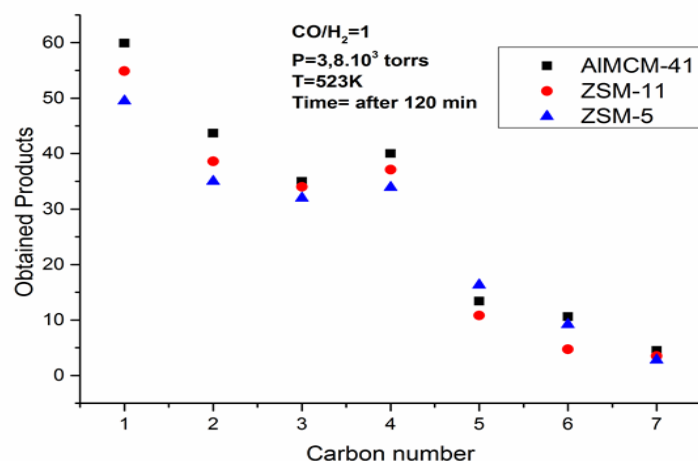


Fig. 8. Distribution of C_1 - C_7 of obtained product on CO hydrogenation over different Pt^{n+}/H^+ -catalyst after 120min at 523K, $P=1,2$ MPa, $CO/H_2=1$.

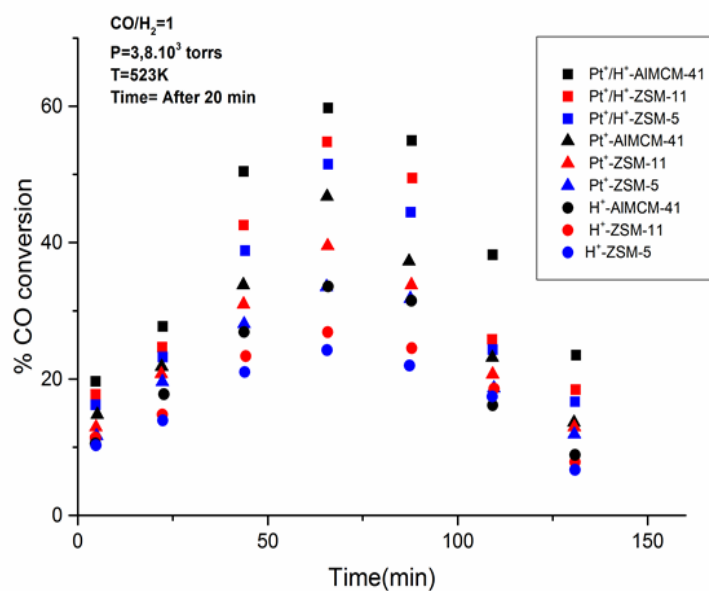


Fig. 9. CO hydrogenation versus time-on-stream for different exchanged catalysts at 523K, $P=1,2$ MPa, $CO/H_2=1$.

mesoporous catalysts. Mesoporous material structures support the formation of multi-branched fractions. It is well known that alkene reactivity on acid catalysts increases with increasing carbon number and varies differently with catalysts. For extended periods of time on stream, more significant changes could be predicted in heavier fractions. Double bond shift reactions occur easily over molecular sieves. Therefore, 1-alkenes with high selectivity were observed for zeolites ZSM-11 and ZSM-5. But in the case of mesoporous, the *cis* and *trans* proportions (branched) alkenes were higher.

3.4. Effect of time on stream

The obtained products with the variation of time-on-stream were higher for catalysts exchanged with combined ions (Fig. 9). Then, significant differences in product selectivities were observed for different exchanged solids. The C_1 - C_7 hydrocarbon distribution (Fig. 8) showed a decrease in the amount of C_1 , C_4 and C_5 hydrocarbons. Moreover, a slight increase in C_3 products was observed. Even after 70 min on stream, the tendency was similar for all catalysts, with an important decrease in the amount of obtained products for catalysts exchanged only with platinum and platinum/ammonium, and a slight increase for those exchanged with ammonium. This phenomenon was

most likely caused by the acidity of the first series of catalysts, which facilitates their deactivation in contrast to the second catalyst series (Fig. 10).

Hydrocarbon fractions were lower with relatively high iso/n-alkane of C₄ and only n-Alkanes of C₂ (Fig. 5). As mentioned above, propylene transformed within catalysts gives low C₃H₄/C₃H₈ ratios and a diminution in the C₃ fraction. The hydrogen transfer mechanism on reactive surfaces has a direct impact on this reaction type. Then, the variation of time on stream allows a chain growth mechanism with a notable decrease in products due to the deactivation phenomenon. The iso-/n-alkanes ratios corresponding to the C₂ and C₅ fractions were similarly found to be greater for catalysts exchanged (Ptⁿ⁺ and/or H⁺)-catalysts than for H-catalysts and this tendency was in an inverse proportion to time on stream (Fig. 11a, b). These findings imply that alkenes were generated by secondary reactions such as cracking, isomerization oligomerization and hydrogen transfer in the presence of AIMCM-41 mesoporous solid. The presence of different ion types exchanged different states of valences of metals, and their distribution in these solids shifted the most for C₄ and C₆. As a consequence, owing to a higher density of acid sites, important secondary reactions were observed.

During the first 20 minutes of the stream, zeolites became deactivated more easily and quickly than AIMCM-41 materials due to their structure and texture. The C₁-C₇ distribution, alkenes/alkanes, and iso-/n-hydrocarbons ratios were similar to those found in Fischer-Trops reactions with increasing time-on-stream.

3.5. Hydrocarbons selectivity

The CO₂ selectivities, obtained after 15 min on stream, were determined according to the formula cited above. Values corresponding to these selectivities varied between 10 and 40%, depending, on conversion rates (Fig. 12).

$$\frac{\text{Moles C}_n \times n}{\text{Total Moles of C Formed as Products}} \quad [7]$$

The selectivities for linear C₁-C₇ hydrocarbons for AIMCM-41 materials were higher than those of zeolites. The tendency observed has been reported previously [33, 34]. The increase in lighter hydrocarbon selectivities is attributed to several effects like alcohols formation, Cracking of long-chain hydrocarbons and conversion of alkenes on different acid sites [35].

Formed alkenes seem to participate in re-adsorption and chain growth phenomena [36]. Oxygenated products can also be formed from alkenes like hydroformylation reactions. Since catalysts can intercept alkenes, this leads to an increase in light hydrocarbon proportions. ¹³C NMR and liquid phase IR analysis, with values of around 174 ppm and 258 ppm, and 2061-2071 cm⁻¹ and 1855-1869 cm⁻¹, respectively, confirmed the formation of oxygenated products [37]. Greater hydrocarbon varieties, which included branched hydrocarbons, were also detected, especially in the case of mesoporous materials [33]. High-molecular weight hydrocarbons were more observed at the reactor exit with AIMCM-41 than with ZSM-5 and ZSM-11 zeolites. These effects of lowering high-molecular-weight hydrocarbons while increasing methane creation can result in high selectivities for fuel formation.

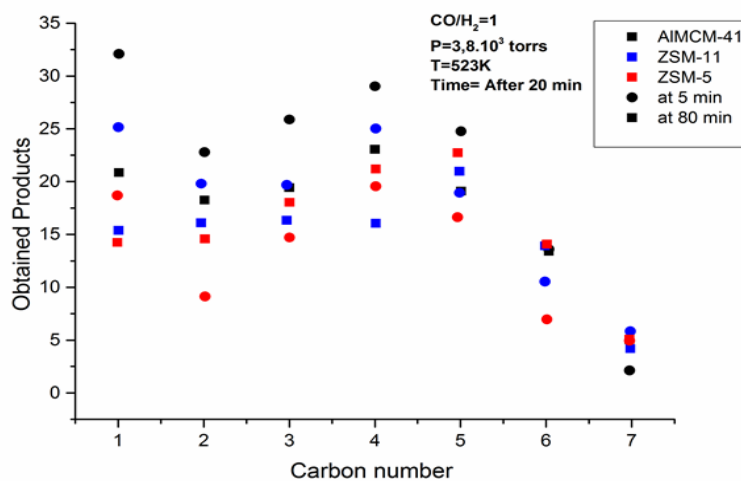


Fig. 10. Hydrocarbon distribution for CO conversion on different Ptⁿ⁺/H⁺-catalysts after 5 min and 80 min on stream at 523K, P=1,2 MPa, CO/H₂=1.

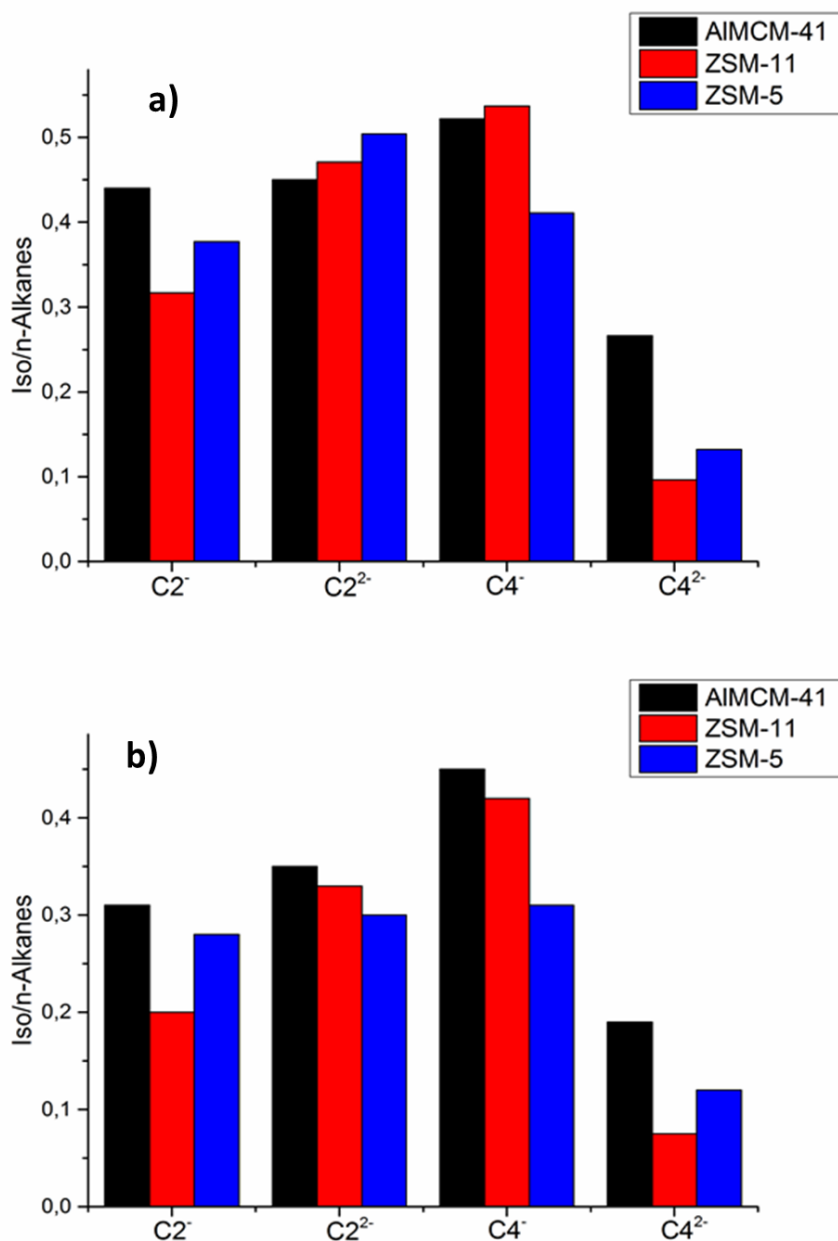


Fig. 11 a) C₂ and C₄ Iso/normal ratios for hydrogenation of CO on different Ptⁿ⁺/H⁺-catalysts s after 5 min on stream at 523K, P=1,2 MPa, CO/H₂=1 **b)** C₂ and C₄ Iso/normal ratios for hydrogenation of CO on different Ptⁿ⁺/H⁺-catalysts s after 2hours on stream at 523K, P=1,2 MPa, CO/H₂=1.

The highest selectivities of C₂-C₄ fractions were obtained easily with different exchanged catalysts in varied proportions (**Fig. 12**) [6, 38]. Again, the participation of factors like types of ions and their dispersion manners inside catalysts and the structure and texture of catalysts could be invoked.

4. Conclusions

The ions-solids formations have an impact on catalytic behavior. The activity of (Ptⁿ⁺/H)-catalysts was higher

compared to Ptⁿ⁺-catalysts or H-catalysts due to the presence of both Bronsted and Lewis acid sites in the inner surfaces of catalysts and their uniform distribution. The Pt²⁺ and Pt⁴⁺ oxidation states did not reveal a significant impact on the course of CO hydrogenation. After the reduction-carburization pre-treatment and the conversion reaction, some platinum in AIMCM-41 remained in the ionic state. Conversion of alkenes generated in this reaction type is favored by acidic characteristics, which were more evident in

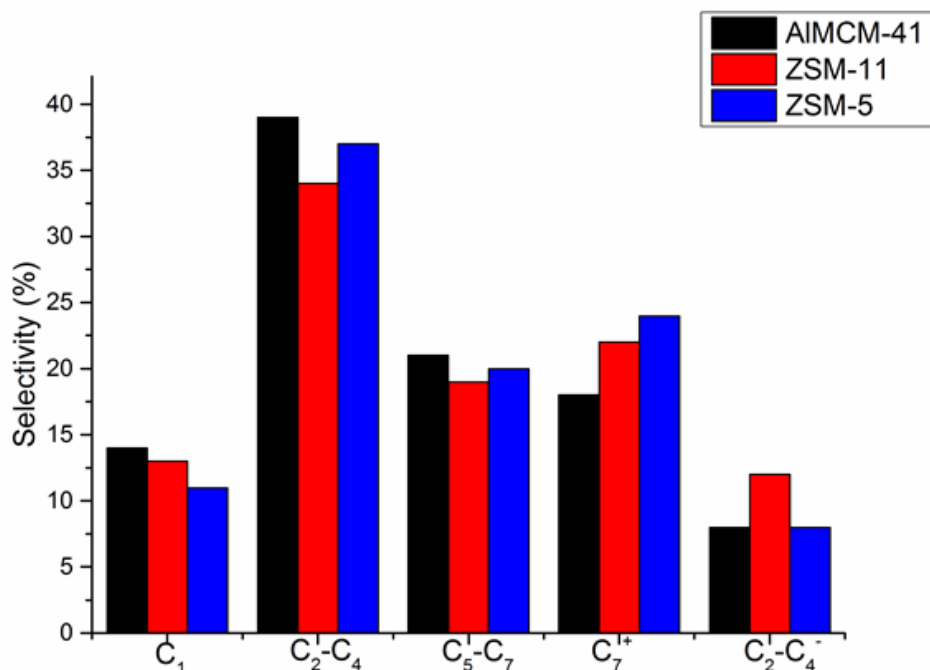


Fig. 12. Selectivities CO₂ free for CO hydrogenation with different Ptⁿ⁺/H⁺-catalysts after 2 hours on stream at 523K, P=1,2 MPa, CO/H₂=1.

Ptⁿ⁺/H⁺-materials than in other mono-exchanged catalysts. Greater conversion activity for the obtained carbon number could be linked to a higher ionic proportion. Different selectivities, solid acidities, as well as structure and texture (zeolites and zeotypes) could explain differences in product distribution observed for different catalysts.

The distribution of CO hydrogenation products is affected by ion combinations within catalysts. In the presence of zeolites, formed alkenes underwent secondary reactions such as cracking, skeletal isomerization, oligomerization, and hydrogen transfer. Skeletal and double bond shift isomerizations were favored in the case of mesoporous AIMCM-41 sieves. According to an analysis of the lighter hydrocarbon fraction, deactivation of acid sites with time-on-stream occurred more strongly with platinum or Ptⁿ⁺/H-catalysts and a deactivation of the reaction was noticed after 70 min on the catalysts which is mainly due to the deposit of cokes and obstruction of the pores. Furthermore, the absence of Pt-O products on FTIR confirms the catalyst results obtained for this reaction of CO hydrogenation. The interaction of solids with various ions, as well as their combination, appears to have a role in CO transformation, resulting in a stronger selectivity for light products such as C₂-C₄ and C₂/iso-C₄.

Selectivity was shown to be more dependent on some factors like the structure of support (ZSM-5, ZSM-11, or AIMCM-41), elements (Ptⁿ⁺ and/or H⁺) introduced within catalysts, the distribution of acidic sites, and acidity strength inside catalysts. Some analogies in product selectivities were observed for catalysts with similar structures (ZSM-5 and ZSM-11). In terms of catalytic behavior, when acid sites began to deactivate for the first time in the stream, CO conversion and selectivity were different due to the presence of the same elements with different structures. On the other hand, CO conversion and selectivity were close for ZSM-11 and ZSM-5 due to their similar structures but different elements. Changes in product selectivity for different materials could be linked to increased acidity and fewer constraints owing to the form of selectivity for ZSM-5, ZSM-11 versus AIMCM-41.

Acknowledgements

We thank the General Directorate of Scientific Research and Technological Development of Algeria (DGRSDT) for its help in carrying out this research work.

References

- [1] A.M. Kovalskii, I.N. Volkov, N.D. Evdokimenko, O.P. Tkachenko, D. V. Leybo, I. V. Chepkasov, Z.I. Popov, A.T. Matveev, A. Manakhov, E.S.

- Permyakova, A.S. Konopatsky, A.L. Kustov, D. V. Golberg, D. V. Shtansky, Hexagonal BN- and BNOsupported Au and Pt nanocatalysts in carbon monoxide oxidation and carbon dioxide hydrogenation reactions, *Appl. Catal. B Environ.* 303 (2022) 120891.
- [2] H.R. Azizi, A.A. Mirzaei, R. Sarani, M. Kaykhahi, Pilot scale study of Co-Fe-Ni nanocatalyst for CO hydrogenation in Fischer-Tropsch synthesis, *Iran. J. Catal.* 9 (2019) 223–231.
- [3] A.K. Datye, M. Votsmeier, Opportunities and challenges in the development of advanced materials for emission control catalysts, *Nat. Mater.* 20 (2021) 1049–1059.
- [4] A.J.M. Miller, J.A. Labinger, J.E. Bercaw, Homogeneous CO hydrogenation: Ligand effects on the lewis acid-assisted reductive coupling of carbon monoxide, *Organometallics.* 29 (2010) 4499–4516.
- [5] F. Studt, F. Abild-Pedersen, Q. Wu, A.D. Jensen, B. Temel, J.D. Grunwaldt, J.K. Norskov, CO hydrogenation to methanol on Cu-Ni catalysts: Theory and experiment, *J. Catal.* 293 (2012) 51–60.
- [6] J. Yang, W. Ma, D. Chen, A. Holmen, B.H. Davis, Fischer-Tropsch synthesis: A review of the effect of CO conversion on methane selectivity, *Appl. Catal. A Gen.* 470 (2014) 250–260.
- [7] V.R.R. Pendyala, W.D. Shafer, G. Jacobs, B.H. Davis, Fischer-Tropsch synthesis: Effect of reaction temperature for aqueous-phase synthesis over a platinum promoted Co/alumina catalyst, *Catal. Letters.* 144 (2014) 1088–1095.
- [8] C. Janke, M.S. Duyar, M. Hoskins, R. Farrauto, Catalytic and adsorption studies for the hydrogenation of CO₂ to methane, *Appl. Catal. B Environ.* 152–153 (2014) 184–191.
- [9] M. Athariboroujny, A. Raub, V. Iablokov, S. Chenakin, L. Kovarik, N. Kruse, Competing Mechanisms in CO Hydrogenation over Co-MnOx Catalysts, *ACS Catal.* 9 (2019) 5603–5612.
- [10] Y.T. Tsai, X. Mo, A. Campos, J.G. Goodwin, J.J. Spivey, Hydrotalcite supported Co catalysts for CO hydrogenation, *Appl. Catal. A Gen.* 396 (2011) 91–100.
- [11] C. Göbel, S. Schmidt, C. Froese, Q. Fu, Y.T. Chen, Q. Pan, M. Muhler, Structural evolution of bimetallic Co-Cu catalysts in CO hydrogenation to higher alcohols at high pressure, *J. Catal.* 383 (2020) 33–41.
- [12] S. Sang, F. Chang, Z. Liu, C. He, Y. He, L. Xu, Difference of ZSM-5 zeolites synthesized with various templates, *Catal. Today.* 93–95 (2004) 729–734.
- [13] M. Sakmeche, A. Belhakem, R. Kessas, S.A. Ghomari, Effect of parameters on NO reduction by methane in presence of excess O₂ and functionalized AlMCM-41 as catalysts, *J. Taiwan Inst. Chem. Eng.* 80 (2017) 333–341.
- [14] Q. Yu, C. Cui, Q. Zhang, J. Chen, Y. Li, J. Sun, C. Li, Q. Cui, C. Yang, H. Shan, Hierarchical ZSM-11 with intergrowth structures: Synthesis, characterization and catalytic properties, *J. Energy Chem.* 22 (2013) 761–768.
- [15] G. Xu, J. Zhang, S. Wang, Y. Zhao, X. Ma, Effect of thermal pretreatment on the surface structure of PtSn/SiO₂ catalyst and its performance in acetic acid hydrogenation, *Front. Chem. Sci. Eng.* 10 (2016) 417–424.
- [16] H. Yoshida, S. Nonoyama, Y.Y.T. Hattori, Quantitative Determination of Platinum Oxidation State by XANES Analysis, *Phys. Scr. T115* (2005) 813-815.
- [17] G. Jacobs, U.M. Graham, E. Chenu, P.M. Patterson, A. Dozier, B.H. Davis, Low-temperature water-gas shift: Impact of Pt promoter loading on the partial reduction of ceria and consequences for catalyst design, *J. Catal.* 229 (2005) 499–512.
- [18] S.K. Das, P. Mohanty, S. Majhi, K.K. Pant, CO-hydrogenation over silica supported iron based catalysts: Influence of potassium loading, *Appl. Energy.* 111 (2013) 267–276.
- [19] A. Belhakem, *Journal of, Asian J. Chem.* 26 (2014) 6745–6750.
- [20] A. Soualah, J.L. Lemberton, L. Pinard, M. Chater, P. Magnoux, K. Moljord, Hydroconversion of n-decane on Pt/HZSM-5 bifunctional catalysts: Effect of the Si/Al ratio of the zeolite on selectivities, *React. Kinet. Mech. Catal.* 101 (2010) 209–219.
- [21] M.W. Kadi, A. Hameed, R.M. Mohamed, I.M.I. Ismail, Y. Alangari, H.M. Cheng, The effect of Pt nanoparticles distribution on the removal of cyanide by TiO₂ coated Al-MCM-41 in blue light exposure, *Arab. J. Chem.* 12 (2019) 957–965.
- [22] M. Sakmeche, A. Belhakem, S.A. Ghomari, L. Belgacem, Hydroconversion of n-C₁₀ alkanes using functionalized AlMCM-41 as catalysts, *React. Kinet. Mech. Catal.* 129 (2020) 975–990.
- [23] M.A. Vannice, J.E. Benson, M. Boudart, Determination of surface area by chemisorption: Unsupported platinum, *J. Catal.* 16 (1970) 348–356.
- [24] R.F. Hicks, A.T. Bell, Effects of metal-support interactions on the hydrogenation of CO over Pd SiO₂ and Pd La₂O₃, *J. Catal.* 90 (1984) 205–220.
- [25] B. Sun, G. Yu, J. Lin, K. Xu, Y. Pei, S. Yan, M. Qiao, K. Fan, X. Zhang, B. Zong, A highly selective Raney Fe@HZSM-5 Fischer-Tropsch synthesis

- catalyst for gasoline production: One-pot synthesis and unexpected effect of zeolites, *Catal. Sci. Technol.* 2 (2012) 1625–1629.
- [26] M. Popova, P. Djinović, A. Ristić, H. Lazarova, G. Dražić, A. Pintar, A.M. Balu, N.N. Tušar, Vapor-Phase Hydrogenation of Levulinic Acid to γ -valerolactone Over Bi-Functional Ni/HZSM-5 Catalyst, *Front. Chem.* 6 (2018) 1–12.
- [27] M. V. Cagnoli, N.G. Gallegos, A.M. Alvarez, J.F. Bengoa, A.A. Yeramián, M. Schmal, S.G. Marchetti, Catalytic CO hydrogenation on potassic Fe/zeolite LTL, *Appl. Catal. A Gen.* 230 (2002) 169–176.
- [28] D.L. Trimm, I.O.Y. Liu, N.W. Cant, The effect of carbon monoxide on the oligomerization of acetylene in hydrogen over a Ni/SiO₂ catalyst, *J. Mol. Catal. A Chem.* 307 (2009) 13–20.
- [29] H. Feng, C. Li, H. Shan, In-situ synthesis and catalytic activity of ZSM-5 zeolite, *Appl. Clay Sci.* 42 (2009) 439–445.
- [30] A. Belhakem, A. Bengueddach, Catalytic properties and acidity of modified MCM-41 mesoporous materials with low Si/Al ratio: Heptane isomerisation, *Bull. Chem. Soc. Ethiop.* 20 (1) (2006) 99-112.
- [31] V.Schunemann, al, Fe Promoted Rh-Clusters in zeolite NaY: Characterization and Catalytic Performance in CO Hydrogenation, *J. Catal.* 153 (1995) 144–157.
- [32] W. Chen, Y. Ding, X. Song, T. Wang, H. Luo, Promotion effect of support calcination on ethanol production from CO hydrogenation over Rh/Fe/Al₂O₃ catalysts, *Appl. Catal. A Gen.* 407 (2011) 231–237.
- [33] J. Panpranot, J.G. Goodwin Jr., A. Sayari, CO Hydrogenation on Ru-Promoted Co/MCM-41 Catalysts, *J. Catal.* 211 (2002) 530–539.
- [34] N. Bungane, C. Welker, E. Van Steen, J.R. Moss, M. Claeys, Osmium Complexes, 63 (2008) 289–292.
- [35] L. Zhang, X. Zhang, K. Qian, Z. Li, Y. Cheng, L.L. Daemen, Z. Wu, W. Huang, Activation and surface reactions of CO and H₂ on ZnO powders and nanoplates under CO hydrogenation reaction conditions, *J. Energy Chem.* 50 (2020) 351–357.
- [36] R. Joshi, A. Saxena, R. Gounder, Mechanistic insights into alkene chain growth reactions catalyzed by nickel active sites on ordered microporous and mesoporous supports, *Catal. Sci. Technol.* 10 (2020) 7101–7123.
- [37] J.P.hindermann, al, Mechanistic Aspects of the Formation of Hydrocarbons and Alcohols from CO Hydrogenation, *Catal. Rev. Sci. Eng.* 35 (2006) 1–127.
- [38] L. Gucci, G. Stefler, O. Geszti, Z. Koppány, Z. Kónya, É. Molnár, M. Urbán, I. Kiricsi, CO hydrogenation over cobalt and iron catalysts supported over multiwall carbon nanotubes: Effect of preparation, *J. Catal.* 244 (2006) 24–32.